

SOLUTION OF SINGULAR ELLIPTIC PDES ON A UNION OF RECTANGLES USING SINC METHODS*

MICHAEL H. HOHN[†]

Abstract. The numerical solution of problems with singularities presents special difficulties for most methods. Adjustments to standard methods are typically made for only a special type of singularity, usually known a priori. The family of sinc numerical methods is naturally suited for general singular problems. Here, the methods are extended and applied to two-dimensional, elliptic first-order systems of mixed boundary value problems with singularities of the form x^α .

Key words. elliptic, PDE, sinc methods, singular problems, BVP

AMS subject classifications. 65N35, 65N12, 74S25, 74G15, 74G70

1. Introduction. The work presented here was motivated by the need for accurate numerical solutions to problems in fracture mechanics. The equations involved are

$$\begin{aligned}(-2\nu + 2) \frac{\partial^2 u^1}{(\partial \theta^1)^2} + (1 - 2\nu) \frac{\partial^2 u^1}{(\partial \theta^2)^2} + \frac{\partial^2 u^2}{\partial \theta^1 \partial \theta^2} &= 0 \\(1 - 2\nu) \frac{\partial^2 u^2}{(\partial \theta^1)^2} + (-2\nu + 2) \frac{\partial^2 u^2}{(\partial \theta^2)^2} + \frac{\partial^2 u^1}{\partial \theta^1 \partial \theta^2} &= 0\end{aligned}$$

with general mixed boundary conditions. The geometry for the cases of interest can be reduced to a union of rectangles in 2D or a union of slabs in 3D.

The difficulty arises from the geometry of these problems: one or more reentrant corners, usually cracks. For crack problems and other problems with corner or edge singularities it is common to combine special local solutions with finite elements or finite differences to handle these singularities. There are many such special-case solutions for very specific boundary conditions and geometries, but their derivations are very involved. For more complex problems, these special solutions are not available because one does not in general know the behavior of the singularity a priori.

However, the locations of the singularities are known, and for most problems solved to date, the singularities are algebraic and have the form $r^\alpha f(\theta)$, $0 < \alpha$, with $f(\theta)$ a smooth function. This makes sinc methods natural candidates for the solution of these problems. In one dimension, this family of methods approximates functions with endpoint singularities of the form x^α with an exponential convergence rate $\exp(-d\sqrt{N})$. For two and higher-dimensional problems on a cartesian product grid, corner singularities of the form r^α , with r the radial distance from the corner, are also handled¹. Thus, only the location and class of the singularity are needed, and the solution can be accurately computed.

Mathematically, the class of problems considered here is two-dimensional, linear, variable-coefficient, elliptic first-order systems of partial differential equations and their boundary conditions, with or without corner and/or edge singularities, defined on a finite connected union of rectangles. On each rectangle, the unknowns' coefficients and the solution are assumed to be smooth; using multiple rectangles, piecewise smooth systems can be solved.

*Received August 31, 2005. Accepted for publication January 29, 2006. Recommended by F. Stenger.

[†]Lawrence Berkeley Laboratory, 1 Cyclotron Road, Mail-Stop 64-246, Berkeley, CA 94720 (mhohn@lbl.gov).

¹ For a problem specified on a union of bounded rectangles. Semi-infinite regions can also be used, but these are not further addressed here.

The method of solution is based on the collocation of a sinc-series representation of the first-order systems, and is henceforth referred to as the SINC-ELLPDE method. It is based on one-dimensional results proven in [5], [6]; these were extended for the present class of problems in [3].

The remainder of this paper proceeds as follows. Basic definitions and a summary of relevant one-dimensional properties of sinc series are presented, followed by a full description of the collocation algorithm, illustrated using a simple abstract example. The theorem justifying this algorithm for two-dimensional approximation is next, presenting the key idea of uniform approximation of unbounded derivatives on a subset of the original domain. A numerical example is used to demonstrate the numerical convergence properties of the method, including a standard norm-based error and the uniform error. A practical method for expressing the uniform absolute error bound is illustrated last.

2. Sinc Method Basics. DEFINITION 2.1 ($\mathcal{D}_d, \mathcal{D}, \phi, \psi$). Pick $d > 0$ and define the strip \mathcal{D}_d by

$$\mathcal{D}_d = \{w \in \mathbf{C} : |\Im w| < d\}$$

Given a region \mathcal{D} containing a contour Γ in \mathbf{C} with endpoints a and b on the boundary of \mathcal{D} , ϕ is a one-to-one conformal map with the properties $\phi : \Gamma \rightarrow \mathbf{R}$, $\phi(x) \rightarrow -\infty$ as $x \rightarrow a$, $\phi(x) \rightarrow \infty$ as $x \rightarrow b$ and $\phi : \mathcal{D} \rightarrow \mathcal{D}_d$

Define $\psi \equiv \phi^{-1}$; then the region \mathcal{D} is the image

$$\mathcal{D} = \psi(\mathcal{D}_d)$$

The functions $\phi(x) = \ln(x - a)/(b - x)$ and $\psi(z) = (\exp(z)b + a)/(\exp(z) + 1)$ map the interval $[a, b]$ to \mathbf{R} and back; they are the ones used in the remainder of this work. Many other maps are available; see [6], Section 1.7.

DEFINITION 2.2 (ρ, L_α). For the region $S_d = \{z \in \mathbf{C} : |\arg z| < d\}$, the map $\rho : \mathcal{D} \rightarrow S_d$ is defined as

$$\rho(z) = e^{\phi(z)}$$

Notice that for $z \in \mathbf{R}$, $\rho : \Gamma \rightarrow [0, \infty)$. Given $\alpha > 0$, $d > 0$ and a region \mathcal{D} , denote by L_α the family of all functions $F(z)$ analytic and uniformly bounded in \mathcal{D} so that $\forall z \in \mathcal{D}$,

$$|F(z)| \leq \frac{C|\rho(z)|^\alpha}{|1 + \rho(z)|^{2\alpha}}$$

for some $C > 0$.

On \mathbf{R} using $\phi(z) = z$, this criterion is

$$|F(z)| \leq \frac{C|e^z|^\alpha}{|1 + e^z|^{2\alpha}}$$

so as $z \rightarrow \infty$, $|F(z)| \leq C_1|e^{-\alpha z}|$ and as $z \rightarrow -\infty$, $|F(z)| \leq C_2|e^{\alpha z}|$ and L_α is the class of exponentially decaying functions.

On $[a, b]$ using $\phi(z) = \ln(z - a)/(b - z)$,

$$|F(z)| \leq C \left| \frac{z - a}{b - z} \right|^\alpha \left| \frac{b - z}{b - a} \right|^{2\alpha}$$

so as $z \rightarrow a^+$, $|F(z)| \leq C_1|z - a|^\alpha$ and as $z \rightarrow b^-$, $|F(z)| \leq C_2|b - z|^\alpha$, so algebraic decay near the endpoints is required of L_α functions in this case.

DEFINITION 2.3 (M_α). Let $\alpha \in (0, 1]$ and $d \in (0, \pi)$. Define f as

$$f = g - \left[\frac{(b - z)g(a) + (z - a)g(b)}{b - a} \right]$$

Then $M_\alpha(\mathcal{D})$ denotes the family of functions g analytic and uniformly bounded in \mathcal{D} such that $f \in L_\alpha(\mathcal{D})$

Functions in the $M_\alpha(\mathcal{D})$ class may have nonzero values at the endpoints, and this class is used in the remainder of this work.

Next are the basic elements used for approximation on \mathbf{R} .

DEFINITION 2.4 (Approximation on \mathbf{R}). The sinc function is defined by

$$\text{sinc}(x) = \frac{\sin(\pi x)}{\pi x}$$

For a given $N > 0$, the j^{th} sinc point is given by

$$z_j = \phi^{-1}(jh) = \psi(jh)$$

where the sinc spacing parameter is

$$h = \sqrt{\frac{\pi d}{\alpha N}}$$

Given $N > 0$ the k^{th} sinc series term on \mathbf{R} is defined by

$$\eta_k(x) = \begin{cases} t_L(x) - \sum_{j=-N+1}^N t_L(jh)S(j, x) & k = -N \\ S(k, x) & k \in -N + 1..N - 1 \\ t_R(x) - \sum_{j=-N}^{N-1} t_R(jh)S(j, x) & k = N \end{cases}$$

with

$$t_L(x) = \frac{1}{1 + e^x}$$

$$S(j, x) = \text{sinc}\left(\frac{x - jh}{h}\right)$$

$$t_R(x) = \frac{e^x}{1 + e^x}$$

These definitions are used on a contour Γ via the appropriate conformal map ϕ and the new functions $\omega_k(z)$, defined as follows.

DEFINITION 2.5 (Approximation on Γ). The k^{th} sinc series term on Γ is defined by

$$\omega_k(z) = \eta_k(\phi(z)).$$

3. One-dimensional properties of sinc series. As mentioned in the introduction, sinc series can be used for numerical approximation of many calculus operations. Here, those theorems relevant for collocation of partial differential equations are repeated. Full proofs can be found in [6]. In the following, the norm $\|\cdot\|$ is the maximum norm on Γ , i.e., for $f(z) \in \Gamma$,

$$\|f(z)\| = \max_{z \in \Gamma} |f(z)|$$

and the $(2N + 1)$ -term approximation error is given by

$$(3.1) \quad \epsilon_N = \sqrt{N} e^{-\sqrt{\pi d \alpha N}}$$

THEOREM 3.1 (Interpolation). *If $f \in M_\alpha(\mathcal{D})$, then there exists a constant $C > 0$, independent of N , s.t.*

$$(3.2) \quad \left\| f - \sum_{j=-N}^N f(z_j) \omega_j \right\| \leq C \epsilon_N$$

THEOREM 3.2 (Differentiation). *Let $f \in M_\alpha(\mathcal{D}')$, let μ be any nonnegative integer and if $\mu > 1$, let $(1/\phi)'$ be uniformly bounded in \mathcal{D}' . Then there exists a constant C_μ independent of N such that*

$$(3.3) \quad \left\| \left(\frac{h}{\phi'} \right)^{(k)} \left[f - \sum_{j=-N}^N f(z_j) \omega_j \right] \right\| \leq C_\mu \epsilon_N$$

for $k = 0, 1, \dots, \mu$.

THEOREM 3.3 (Collocation). *Let $f \in M_\alpha(\mathcal{D})$. Let $\mathbf{c} = (c_{-N}, \dots, c_N)^T$ be a complex vector such that*

$$\left(\sum_{j=-N}^N |f(z_j) - c_j|^2 \right)^{1/2} < \delta$$

where $\delta > 0$. Then

$$(3.4) \quad \left\| f - \sum_{j=-N}^N c_j \omega_j \right\| < C \epsilon_N + \delta,$$

with C as in (3.2).

THEOREM 3.4 (Operator Inversion). *Given an invertible linear elliptic differential operator L and the linear system*

$$Lu = f,$$

define the vector operator $[u]$ as $[u] = (u(z_{-N}), \dots, u(z_N))^T$ and the matrix $[L]$ as

$$[L]_{ij} = (L\omega_j)(z_i)$$

Let $\mathbf{u} = [u]$, and let \mathbf{c} be a vector satisfying

$$[L]\mathbf{c} = [f] + [\epsilon_u]$$

with ϵ_u proportional to the unit-roundoff error. Then

$$\|\mathbf{u} - \mathbf{c}\| \leq \|[L]^{-1}\| \left\{ \|\epsilon_N\| + \|\epsilon_u\| \right\}.$$

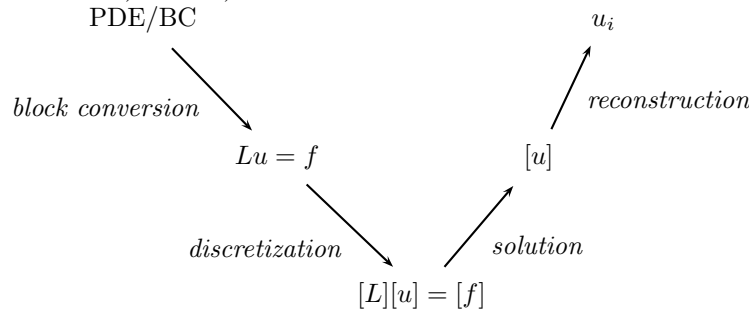
Thus, for $u \in M_\alpha$ and a sufficiently small $\|[L]^{-1}\|$, the computed vector \mathbf{c} satisfies Theorem 3.3 and the solution u can be uniformly computed via

$$(3.5) \quad u \approx \sum_{j=-N}^N c_j \omega_j,$$

with error bound given by (3.4). In Lemma 7.2.5, Section 7.2 of [6], the bound $\|[L]^{-1}\| = O(N^2)$ is derived for a one-dimensional, second-order, linear boundary-value problem under suitable conditions on the coefficients.

4. Collocation Algorithm. This section illustrates the practical collocation procedure via the simplest possible example, Poisson’s equation. Using the preceding definitions, all equations and boundary conditions of a given problem are combined to form a single large linear system which is then discretized; the resulting matrix is solved in one step. The solution of the linear system is obtained via a standard linear system solver, and the individual unknowns’ coefficients extracted. Approximations to the individual unknowns (and their derivatives) can then be computed at non-grid points.

Referring to the following diagram, the detailed steps in sinc collocation are block conversion, discretization, solution, and reconstruction.



Block conversion: For every rectangle, both the PDE and the BCs are written as a collection of first-order systems; in this collection, every unknown is replaced by a sinc series of the form

$$(4.1) \quad \sum_{i=-N_1}^{N_1} \sum_{j=-N_2}^{N_2} c_{ij} \omega_i(x) \omega_j(y);$$

and the corresponding differential operator is applied to this new form.

Discretization: For every rectangle, the resulting collection of systems is then discretized via evaluation of these series at the sinc collocation points

$$(4.2) \quad z_{ij} = (\psi(ih_1), \psi(jh_2)).$$

The discretizations from all rectangles are then combined into one linear system

$$[L][u] = [b]$$

Solution: This linear system is large and sparse, and is solved using a direct sparse linear solver. Generally, accuracy of the linear system solution is limited by the conditioning of the matrix $[L]$, and this conditioning is easily checked by experiment².

Reconstruction: The sets of coefficients c_{ij} , for all unknowns on all rectangles, are then extracted from the resulting solution vector $[u]$ and every original unknown is approximated using a series of the form of (4.1).

Given an unknown f and its sinc series approximation \bar{f} from (4.1), the bound for the absolute error is given in practice by

$$(4.3) \quad \epsilon_N = c\sqrt{N} \exp(-g\sqrt{N})$$

for the function, and by

$$(4.4) \quad \partial\epsilon_N = cN \exp(-g\sqrt{N})$$

for scaled first derivatives, from (3.3).

To better illustrate this approach, the four stages of the algorithm are considered in more detail via an abstract example.

4.1. Block system. As an illustration, a single unknown, single rectangle, second-order elliptic PDE problem can be written in the form $Lu = f$ as

$$(4.5) \quad \begin{pmatrix} L_{1\wedge I}^{1|1} \\ L_{1\wedge T}^{1|1} \\ L_{1\wedge L}^{1|1} \\ L_{1\wedge B}^{1|1} \\ L_{1\wedge R}^{1|1} \end{pmatrix} u^{1|1} = \begin{pmatrix} g_{1\wedge I}^{1|1} \\ g_{1\wedge T}^{1|1} \\ g_{1\wedge L}^{1|1} \\ g_{1\wedge B}^{1|1} \\ g_{1\wedge R}^{1|1} \end{pmatrix}$$

where, using indexing for unknowns and directions, the notation

$$i|j, k$$

denotes unknown i in domain j and direction k . Usually, i or k will be absent. Similarly, the notation

$$i \wedge R$$

denotes equation i in region R , where R is one of I, T, L, B, R, corresponding to the interior and sides of the rectangle. By introducing the new unknowns $u^{11|1}$ and $u^{12|1}$ and the equations

$$\begin{aligned} u^{11|1} &= \partial u^{1|1} / \partial x \\ u^{12|1} &= \partial u^{1|1} / \partial y \end{aligned}$$

²The reciprocal condition number was found to be in the range $10^{-8} - 10^{-12}$ for the problems considered; this is well above the unit-roundoff error for IEEE double precision, $\approx 2.22\text{E-}16$.

all occurrences of second-order partials can be replaced with first-order expressions; omitting blocks of zeroes, the equivalent first-order system then has the form

$$(4.6) \quad \begin{pmatrix} \bar{L}_{1\wedge I}^{1|1} & \bar{L}_{1\wedge I}^{11|1} & \bar{L}_{1\wedge I}^{12|1} \\ \bar{L}_{2\wedge I}^{1|1} & \bar{L}_{2\wedge I}^{11|1} & \\ \bar{L}_{3\wedge I}^{1|1} & & \bar{L}_{3\wedge I}^{12|1} \\ \bar{L}_{1\wedge T}^{1|1} & \bar{L}_{1\wedge T}^{11|1} & \bar{L}_{1\wedge T}^{12|1} \\ \bar{L}_{2\wedge T}^{1|1} & \bar{L}_{2\wedge T}^{11|1} & \\ \bar{L}_{3\wedge T}^{1|1} & & \bar{L}_{3\wedge T}^{12|1} \\ \bar{L}_{1\wedge L}^{1|1} & \bar{L}_{1\wedge L}^{11|1} & \bar{L}_{1\wedge L}^{12|1} \\ \bar{L}_{2\wedge L}^{1|1} & \bar{L}_{2\wedge L}^{11|1} & \\ \bar{L}_{3\wedge L}^{1|1} & & \bar{L}_{3\wedge L}^{12|1} \\ \bar{L}_{1\wedge B}^{1|1} & \bar{L}_{1\wedge B}^{11|1} & \bar{L}_{1\wedge B}^{12|1} \\ \bar{L}_{2\wedge B}^{1|1} & \bar{L}_{2\wedge B}^{11|1} & \\ \bar{L}_{3\wedge B}^{1|1} & & \bar{L}_{3\wedge B}^{12|1} \\ \bar{L}_{1\wedge R}^{1|1} & \bar{L}_{1\wedge R}^{11|1} & \bar{L}_{1\wedge R}^{12|1} \\ \bar{L}_{2\wedge R}^{1|1} & \bar{L}_{2\wedge R}^{11|1} & \\ \bar{L}_{3\wedge R}^{1|1} & & \bar{L}_{3\wedge R}^{12|1} \end{pmatrix} \begin{pmatrix} u^{1|1} \\ u^{11|1} \\ u^{12|1} \end{pmatrix} = \begin{pmatrix} \bar{g}_{1\wedge I}^1 \\ \bar{g}_{1\wedge T}^1 \\ \bar{g}_{1\wedge L}^1 \\ \bar{g}_{1\wedge B}^1 \\ \bar{g}_{1\wedge R}^1 \end{pmatrix}$$

or

$$\bar{L}\bar{u} = \bar{f}$$

4.2. Discrete block system. The discrete block system structure is visually identical to that of the block system; the differences in the blocks come from the discretization, which introduces the unknowns' coefficients and the regions' collocation points. Full details on the ordering of these new parts are not relevant here and a high-level description can proceed as follows. Let $k \in [-N, N]$, $l \in [-N, N]$. Define $m \equiv 2N + 1$, and let $j \in [0, m^2 - 1]$. Define a discrete one-to-one mapping

$$\tau : (k, l) \rightarrow j.$$

In the following, let i be an enumeration of all collocation points of the current appropriate region, and j an enumeration of all coefficients of the current appropriate unknown. Define

$$k_j, l_j = \tau^{-1}(j)$$

and form the following discrete matrix blocks:

$$\left[\bar{L}_{1\wedge I}^{1|1} \right]_{ij} = \left(L_{1\wedge I}^{1|1} \right) (\omega_{k_j}^{1,x} \omega_{l_j}^{1,y})(x_i, y_i), \\ (x_i, y_i) \in I$$

$$\begin{aligned} \left[L_{1 \wedge T}^{1|1} \right]_{ij} &= \left(L_{1 \wedge T}^{1|1} \right) (\omega_{k_j}^{1,x} \omega_{l_j}^{1,y})(x_i, y_i), \\ &(x_i, y_i) \in T \end{aligned}$$

$$\begin{aligned} \left[L_{1 \wedge L}^{1|1} \right]_{ij} &= \left(L_{1 \wedge L}^{1|1} \right) (\omega_{k_j}^{1,x} \omega_{l_j}^{1,y})(x_i, y_i), \\ &(x_i, y_i) \in L \end{aligned}$$

$$\begin{aligned} \left[L_{1 \wedge B}^{1|1} \right]_{ij} &= \left(L_{1 \wedge B}^{1|1} \right) (\omega_{k_j}^{1,x} \omega_{l_j}^{1,y})(x_i, y_i), \\ &(x_i, y_i) \in B \end{aligned}$$

$$\begin{aligned} \left[L_{1 \wedge R}^{1|1} \right]_{ij} &= \left(L_{1 \wedge R}^{1|1} \right) (\omega_{k_j}^{1,x} \omega_{l_j}^{1,y})(x_i, y_i), \\ &(x_i, y_i) \in R \end{aligned}$$

$$[g_{1 \wedge m}^1]_i = g_{1 \wedge m}^1(x_i, y_i)$$

$$m \in [I, T, L, B, R]$$

For consistency, define

$$[u^{1|1}]_j = c_{k_j l_j}^{1|1}$$

Then the operator form in (4.5) has the discrete block analogue

$$\begin{pmatrix} \left[L_{1 \wedge I}^{1|1} \right] \\ \left[L_{1 \wedge T}^{1|1} \right] \\ \left[L_{1 \wedge L}^{1|1} \right] \\ \left[L_{1 \wedge B}^{1|1} \right] \\ \left[L_{1 \wedge R}^{1|1} \right] \end{pmatrix} [u^{1|1}] = \begin{pmatrix} [g_{1 \wedge I}^1] \\ [g_{1 \wedge T}^1] \\ [g_{1 \wedge L}^1] \\ [g_{1 \wedge B}^1] \\ [g_{1 \wedge R}^1] \end{pmatrix}$$

or

$$[L][u] = [f]$$

Note that while none of the constituent matrix blocks is square, the matrix $[L]$ is.

By forming discrete matrix blocks for the system of equations (4.6) in the same manner, the operator form of (4.6) has a discrete block analogue so the large sparse linear system

$$[\bar{L}][\bar{u}] = [\bar{f}]$$

is obtained.

4.3. Discrete approximation. It is assumed that the PDE system is well-posed, so the resulting discrete block system is uniquely invertible and numerically nonsingular. Under these assumptions, any stable solution method obtains a vector $[c]$ satisfying

$$(4.7) \quad [\overline{L}][c] = [\overline{f}] + [\overline{\epsilon}_u]$$

with $[\overline{\epsilon}_u]$ proportional to the unit roundoff error.

The system thus obtained is large, sparse, and poorly conditioned, leading naturally to the use of sparse direct solvers³.

4.4. Uniform approximation. Formally using Theorem 3.4 for the vectors u and c , we see that

$$\|[\overline{u}] - [c]\| \leq \|[\overline{L}]^{-1}\| \left\{ \|[\overline{\epsilon}_N]\| + \|[\overline{\epsilon}_u]\| \right\}$$

and Theorem 3.3 therefore applies. The coefficients $[u^{i|j}]$ can thus be extracted from $[c]$ and used to obtain $u^{i|j}(x, y)$ for any $(x, y) \in \Omega_j$ via (3.5); by Theorem 3.2, this introduces the same $O(\epsilon_N)$ error as the discretization steps.

5. Two-dimensional results. The key result needed here is the following theorem. Rectangle i is denoted by Q^i and defined as

$$Q^i = [a^{i,x}, b^{i,x}] \times [a^{i,y}, b^{i,y}]$$

The projection operators are defined by

$$(\mathcal{P}^i f^i)(x, y) = \sum_{k=-N^{i,x}}^{N^{i,x}} \sum_{l=-N^{i,y}}^{N^{i,y}} f^i(x_k^i, y_l^i) \omega_k^{i,x}(x) \omega_l^{i,y}(y)$$

and with appropriate derivatives for $(\mathcal{P}_x^i f^i)$ and $(\mathcal{P}_y^i f^i)$

THEOREM 5.1 (Collocation). *Let $[u]$ be computed by the algorithm in Section 4, and satisfy (4.7). Let \overline{u} denote the exact solution to $L\overline{u} = f$. Then for all $(x, y) \in Q^i$,*

$$(5.1) \quad \left| [\overline{u}^{i|d} - \mathcal{P}^i u^{i|d}](x, y) \right| \leq e^{-\sqrt{\pi d \alpha N}} (C \log^3 N \| [L]^{-1} \| N)$$

Further, let

$$(5.2) \quad [a^{i,x} < a_s^{i,x} < b_s^{i,x} < b^{i,x}]$$

$$(5.3) \quad [a^{i,y} < a_s^{i,y} < b_s^{i,y} < b^{i,y}]$$

and define Q_s^i by

$$Q_s^i = [a_s^{i,x}, b_s^{i,x}] \times [a_s^{i,y}, b_s^{i,y}]$$

Then for all $(x, y) \in Q_s^i$,

$$(5.4) \quad \left| [\overline{u}_x^{i|d} - \mathcal{P}_x^i u_x^{i|d}](x, y) \right| \leq e^{-\sqrt{\pi d \alpha N}} (C \log^3 N \| [L]^{-1} \| N^{3/2}) \left| (\phi^{i,x})'(x) \right|$$

³Here, SUPERLU [2] was used, with the COLAMD ordering algorithm of [1].

and

$$\left| [\bar{u}_y^i]^d - \mathcal{P}_y^i u^i|^d(x, y) \right| \leq e^{-\sqrt{\pi d \alpha N}} (C \log^3 N \| [L]^{-1} \| N^{3/2}) \left| (\phi^{i,y})'(y) \right|$$

This theorem states that unbounded derivatives can be uniformly approximated on a closed subset of the collocation rectangle excluding the edges, and subject to scaling by the conformal map's derivative. In practice, this means that for a chosen accuracy ϵ , increasing N widens the subregion on which this accuracy is obtained. This is illustrated in the next section.

6. A concise example. For illustration, the Laplace equation

$$\nabla^2 u^{1|1} = 0$$

with the Dirichlet boundary condition $u^{1|1} = f(x, y)$ on top, left, and right boundaries, and the Neumann condition $\partial u^{1|1} / \partial y = f_y(x, y)$ on the bottom boundary, is used.

The domain is the unit square $[0, 1] \times [0, 1]$; the conformal map

$$\phi(x) = \ln \frac{(x-a)}{(b-x)}$$

is used in both directions. The inverse

$$\psi(x) = \phi^{-1}(x) = \frac{a + be^x}{e^x + 1}$$

is used in (4.2) to compute the collocation grid.

The exact solution is taken to be the real part of $z \ln(z)$ or

$$f(x, y) = \frac{1}{2} x \ln(x^2 + y^2) - y \arctan(y, x),$$

providing a weakly singular solution and an excellent test for the SINC-ELLPDE method. For this solution, the partials in x and y are

$$f_x(x, y) = \frac{1}{2} \ln(x^2 + y^2) + 1$$

and

$$f_y(x, y) = -\arctan(y, x),$$

respectively. The first-order system form is easily obtained. By defining the additional unknowns $u^{11|1}$ and $u^{12|1}$ as

$$\begin{aligned} u^{11|1} &= \partial u^{1|1} / \partial x \\ u^{12|1} &= \partial u^{1|1} / \partial y, \end{aligned}$$

the second-order equation becomes

$$\partial u^{11|1} / \partial x + \partial u^{12|1} / \partial y = 0$$

The two definitions and this equation form the set of interior equations for domain 1, the only domain (rectangle) for this problem.

To obtain the data for illustration of the sinc convergence rate and general convergence behavior, the discretization, solution, and reconstruction steps are run several times, each time varying only N .

6.1. Data examination. The interpretation of these data in light of Theorem 5.1 and in the presence of the singularity is more complex. To get a simple global view of convergence, the unbounded derivatives and associated unbounded absolute error are impractical. As the p -norms of the absolute error, $1 \leq p < \infty$, all weigh the error by area, they avoid this problem. The common approach of examining the L^1 norm of the absolute error vs. N is therefore sufficient for a global convergence test. This is used in Section 6.2.

More important is the measure of absolute pointwise error when examining singular problems or problems with boundary layers. The maximum norm would show very large absolute errors when in fact only small regions have large errors, while normwise convergence checks give only a global indication of convergence and say nothing about the local quality of approximation. A direct pointwise examination of the data in Section 6.3 illustrates the practical implications of Theorem 5.1. Using these observations and Theorem 5.1, the pointwise error can be expressed using only two numbers, the desired boundary layer width δ_b and the accuracy ϵ_N obtained on the resulting rectangle Q^i . This is illustrated in Section 6.4.

6.2. Convergence in norm. The error bounds of (4.3) and (4.4) are sharper for large N . To get uniform vertical scaling, the logarithms of the error bound, $e_f(N)$, is fitted to the logarithm of the absolute error, $\ln |f - \bar{f}|$. Using a logarithmic scale for (4.3), the error bound for function approximation becomes

$$e_f(N) = (\log(c) + \log(N)/2 - g\sqrt{N})/\log(10)$$

while the scaled derivative error, from (4.4), is bounded by

$$e_{\partial f}(N) = (\log(c) + \log(N) - g\sqrt{N})/\log(10).$$

Figures 6.1, 6.2, and 6.3 show the convergence of u , u_x and u_y , respectively, using the $\log_{10}(|f - \bar{f}|)$ vs. N approach. To avoid the mentioned low- N inaccuracies, the points $N < 15$ were purposely ignored in the curve fits of the theoretical error bounds.

The figures show excellent agreement between the theoretical- and computed errors for $N \geq 15$, confirming the exponential convergence rate. Further, the theoretical value for g is given by $g = \sqrt{\pi d \alpha}$; with the default choices $d = \pi/2$ and $\alpha = 1$, $g \approx 2.22$, which is close to the computed values of 1.89, 2.28, and 2.20, respectively.

6.3. Pointwise convergence. As seen in (5.1), the pointwise convergence for u is uniform across the entire domain.

To provide some insight into the pointwise convergence behavior of u_x over different areas of a given rectangle, the graphs in Figures 6.4 – 6.7 show a paired combination of three-dimensional surface- and two-dimensional xy-plots. The first figure in each pair displays a surface view of the unknown; lines on the surface and their projections onto the base show the location of the xy-slices. The base projections are numbered for cross-reference with the xy-slices' graphs. The second figure shows the detail slices' xy-graphs. Each slice is numbered according to its position on the area/surface view graph.

From (5.4), one expects a very small error in the interior which increases rapidly near the boundaries. Further, for increasing N , the size of the near-boundary region should decrease. As can be seen in Figure 6.5, this does in fact happen. On the range used here – all of the rectangle – the approximation is very good in the interior of the rectangle, but rapidly worsens near the boundaries. For $m = 7$, this near-boundary error reaches quite far into the interior, while for $m = 19$, the error is restricted to a small near-boundary region.

To check this characteristic for increasing N , Figure 6.6 provides a closer look at a small area near $(0, 0)$, using larger values of N . In Figure 6.7, it is seen that for $m = 19$, good accuracy is obtained to about $x = 0.02$, and the accuracy again diminishes when moving

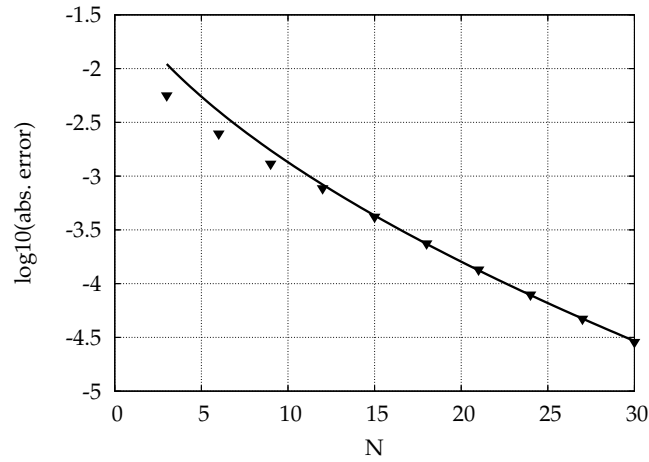


FIG. 6.1. Absolute error as function of N for u . The error is in the L^1 sense. The curve is given by $c\sqrt{N} \exp(-g\sqrt{N})$, with $c = 0.168$ and $g = 1.89$.

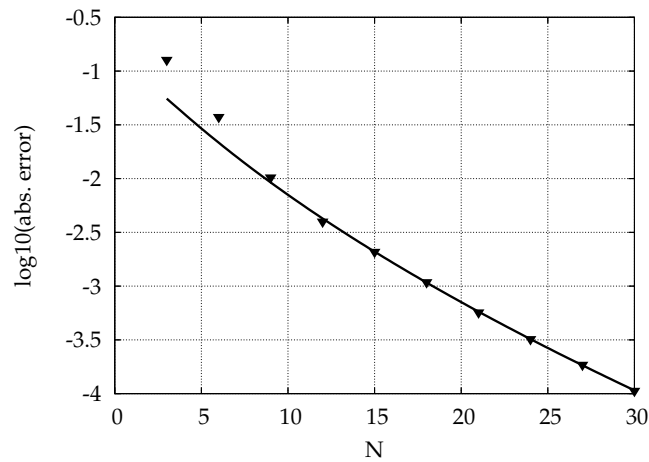


FIG. 6.2. Absolute error as function of N for u_x . The error is in the L^1 sense. The curve is given by $cN \exp(-g\sqrt{N})$, with $c = 0.966$ and $g = 2.28$.

closer to the boundary. Increasing the number of terms from $m = 19$ to $m = 37$ shrinks the inaccurate near-boundary region, as happened on the full rectangle (Figure 6.4) for $m = 7$ and $m = 19$.

Results for u_y are similar and shown more compactly in the following.

6.4. Practical Pointwise Convergence. The behavior described in Theorem 5.1 and observed in the previous section requires a function to describe the uniform error bound; for the y direction, this error envelope is

$$(6.1) \quad E(N, y) = CN^{3/2} \exp(-D\sqrt{N}) \phi'(y)$$

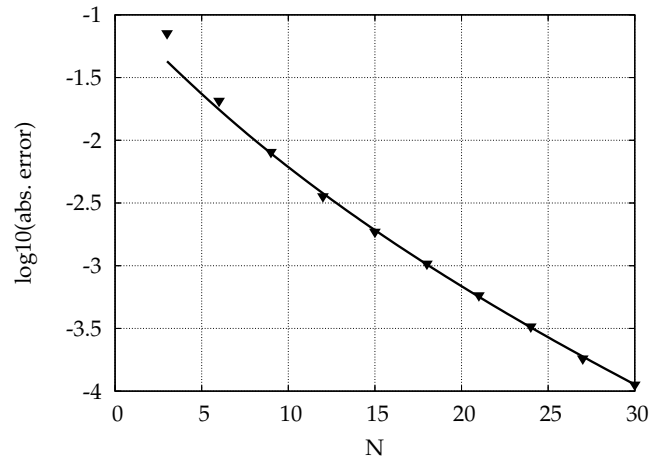


FIG. 6.3. Absolute error as function of N for u_y . The error is in the L^1 sense. The curve is given by $cN \exp(-g\sqrt{N})$, with $c = 0.639$ and $g = 2.20$.

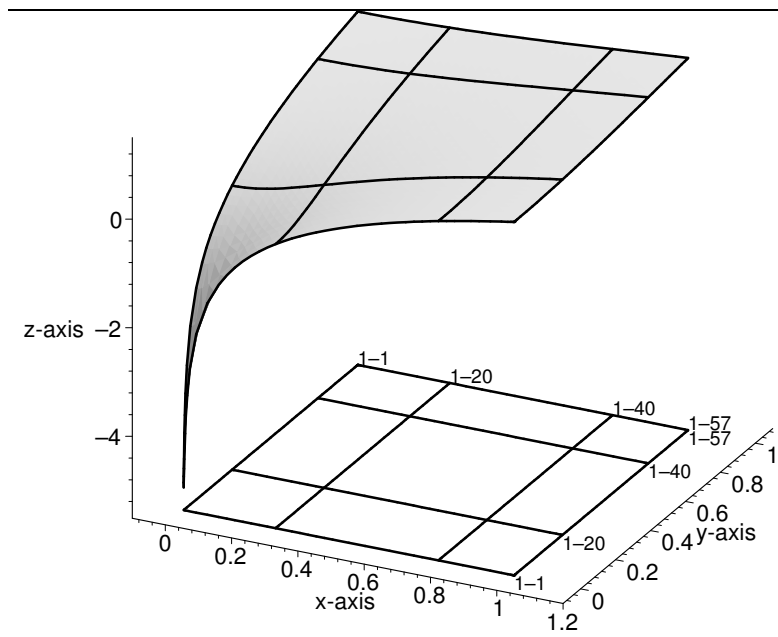


FIG. 6.4. Graph of u_x and slice locations over the whole $[0, 1] \times [0, 1]$ domain. Slices are shown in Figure 6.5.

The absolute error for u and scaled u_y is largest in the center of the domain⁴; as result, $E(N, y)$ is a substantial overestimate along most of the curve. Knowing the maximum error is in the interior, it is trivial to match $E(N, y)$ to the actual error. This was done in Figure 6.8, which shows the absolute errors for $N = 18$ and $N = 24$, and the fitted envelope for each.

Choosing a desired accuracy and distance from the boundary as in Figure 6.9, it is seen

⁴ It is assumed here that the precise edge behavior of the solution u is not known. The blind choice $\alpha = 1$ is a good starting point, but may result in a skewed error distribution, as in this case. If correct values of α and β are available, they can be used in the calculation of the gridpoint spacing to get a more uniform absolute error.

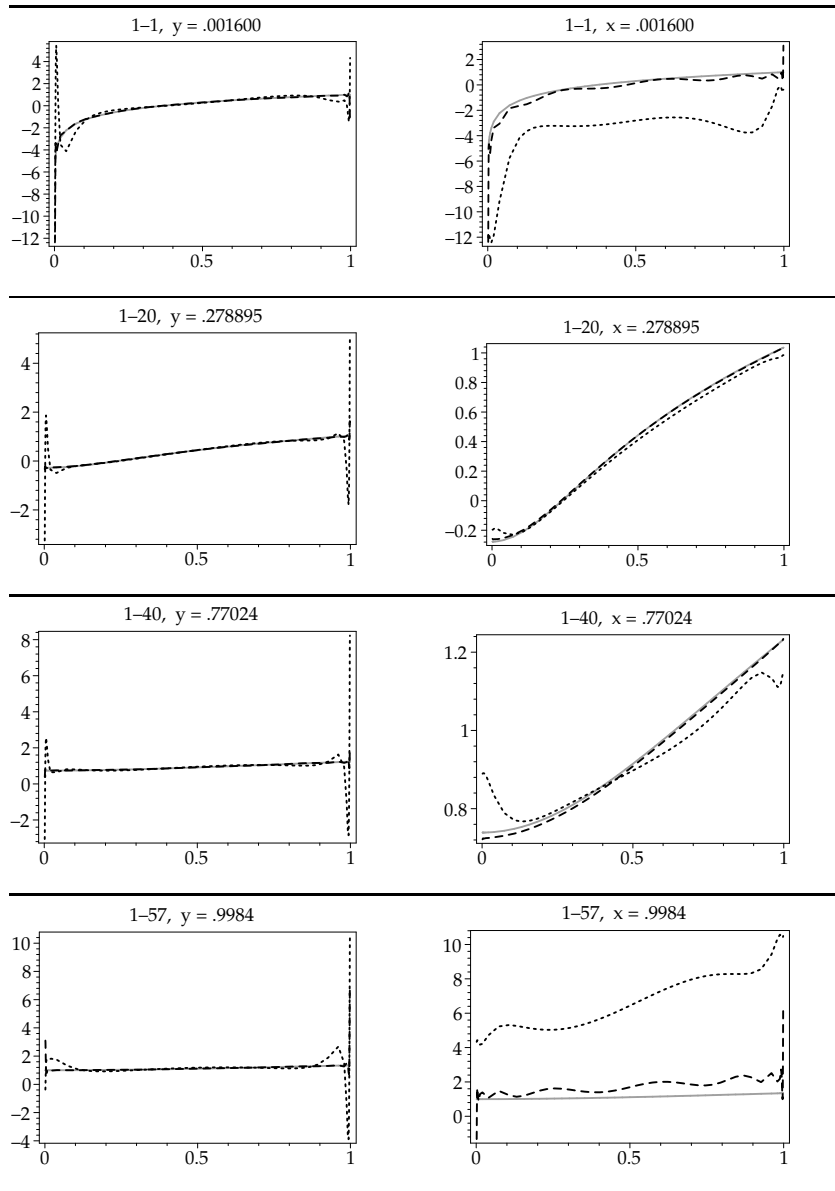


FIG. 6.5. Graphs of slices detailing the pointwise error in the approximation of u_x . The locations of these slices are shown, by index, in Figure 6.4.

that the error envelope rapidly approaches the boundary as N increases. More precisely, the expression for $\partial y / \partial N$, near the singularity and using (6.1) with $E(N, y) = P$ and $\phi'(y) = 1/(y(1-y))$ is

$$\partial y / \partial N \approx \frac{-CNd}{2P} e^{-d\sqrt{N}}$$

so this boundary layer also shrinks at an exponential rate.

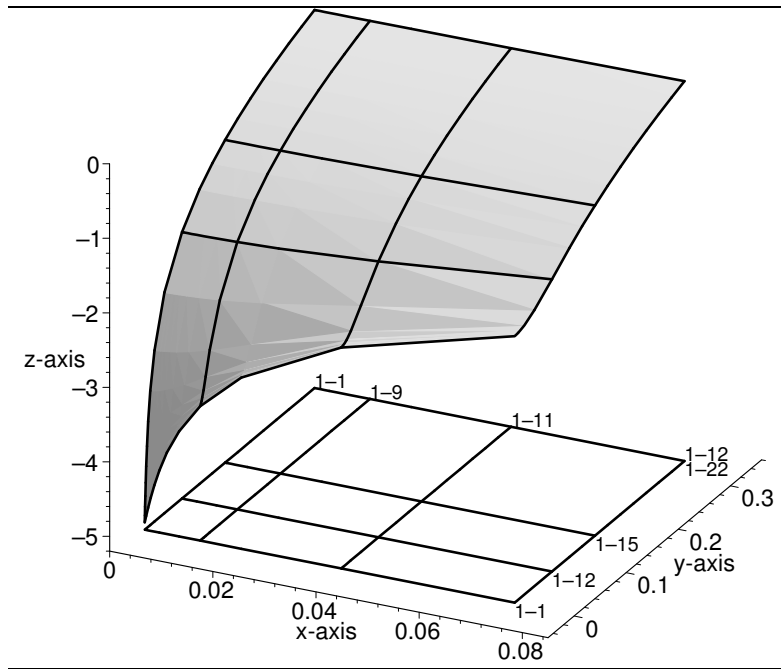


FIG. 6.6. Graph of u_x and slice locations over the $[0, 0.08] \times [0, 0.35]$ subdomain. Slices are shown in Figure 6.7.

The exponential decrease of both error and boundary width thus allows for a simplified convergence test. By choosing the desired boundary layer width δ_b first, a regular convergence curve can again be used, where the uniform absolute error is $E(N, \delta_b)$.

7. Discussion. Theoretical error bounds for sinc methods tend to be overly pessimistic. In practice, the error bound of $C\epsilon_N$ (3.1) is observed in two-dimensional single- and multi-domain problems. Also observed is a strong variation of the solution-dependent C . Perhaps due to coupling effects, C increases with the number of unknowns and number of domains. C also increases for more difficult functions, those with oscillation and stronger singularities. The effect of this is seen in the minimum number of terms required to get useful accuracy. For the simplest functions, $N = 5$ is sufficient for the approximation to resemble the function, between 1 and 2 significant digits. For multi-domain, multiple-unknown problems with corner singularities, 1 to 2 digits of accuracy are not seen until $N = 18$.

Many details were purposely omitted in the preceding presentation. Among these are the conversion of input equations, the intermediate data structures encountered in an implementation of the method, and the full convergence proofs of the method. The manual conversion from equations and boundary conditions to solver input is quite complicated and error prone if done by hand. Because the structure of the equations is very regular, fully automatic conversion from a simple input format to the input to the solver is possible. The details of this conversion algorithm, including automatic production of $\text{T}_{\text{E}}\text{X}$ equations, are described in [4].

The significantly increased complexity of the full proofs contributes little to this presentation, so the reader is referred to chapter 7 of [3] for full details. That reference also contains a full description of the intermediate data structures encountered in discretization and matrix assembly, some discussion of computational effort, and more complex sample problems.

Sinc methods are very broadly applicable; for a concise overview including integration, initial value problems, and some integral equations, see [7]. For a very comprehensive sinc

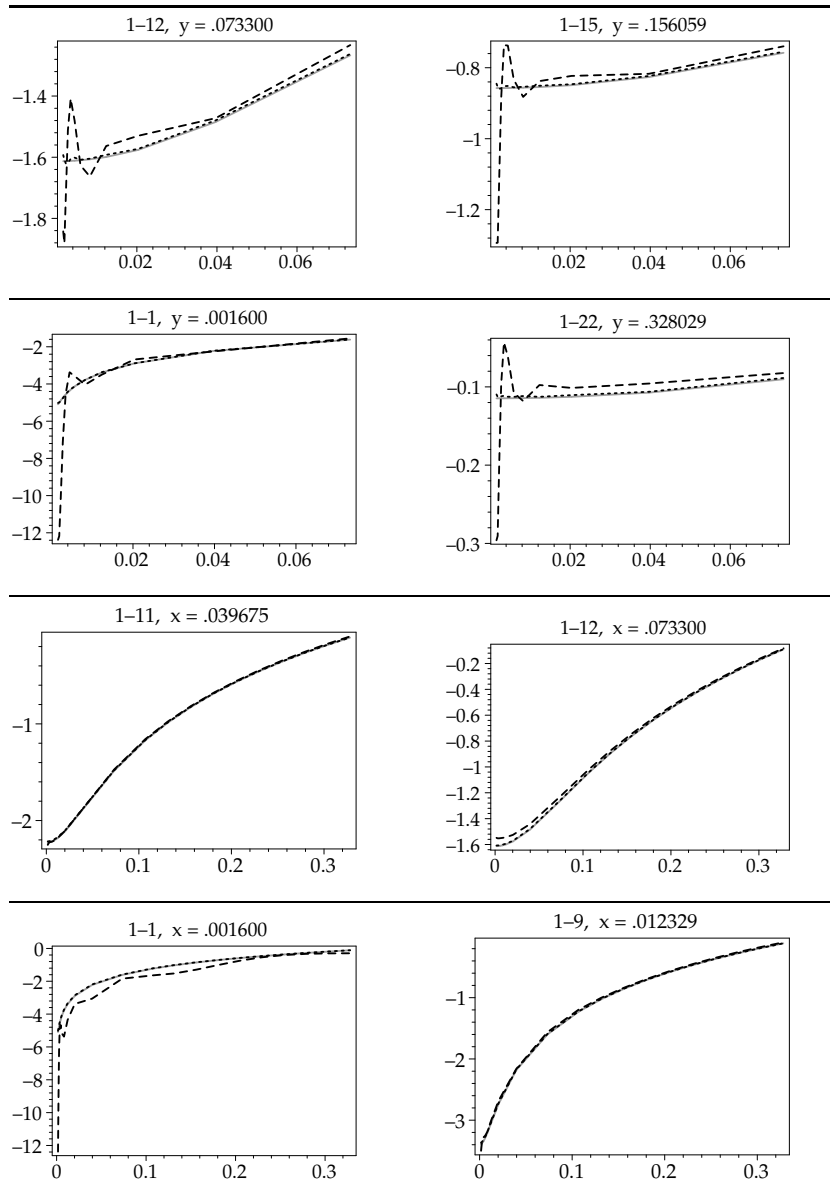


FIG. 6.7. Graphs of slices detailing the pointwise error in the approximation of u_x . The locations of these slices are shown, by index, in Figure 6.6. Legend: Dashed line, $N = 9$. Dotted line, $N = 18$. Solid line, exact.

reference, see [6].

REFERENCES

- [1] T. A. DAVIS, J. R. GILBERT, S. I. LARIMORE, AND E. G. NG, *A column approximate minimum degree ordering algorithm*, ACM Trans. Math. Software, 30 (2004), pp. 353–376.
- [2] J. W. DEMMEL, S. C. EISENSTAT, J. R. GILBERT, X. S. LI, AND J. W. H. LIU, *A supernodal approach*

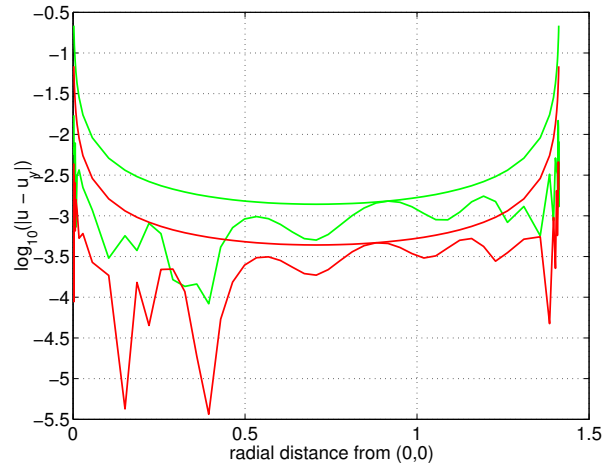


FIG. 6.8. Envelopes and computed errors for $N = 18$ and $N = 24$.

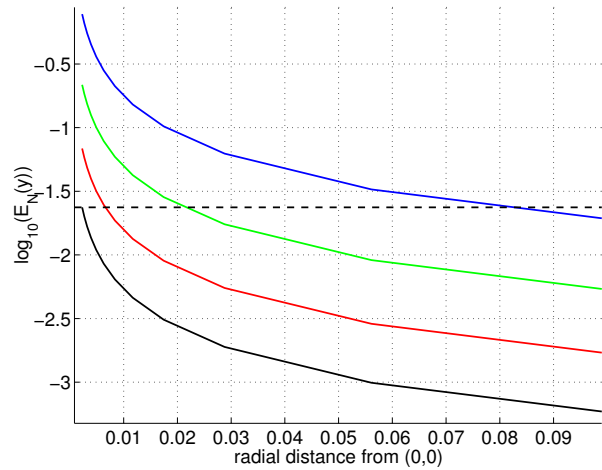


FIG. 6.9. Envelopes approaching boundary for a fixed maximum error (dashed line). Values of N are 12, 18, 24, 30.

to sparse partial pivoting, SIAM J. Matrix Anal. Appl., 20 (1999), pp. 720–755. Implementation and documentation available at <http://www.nersc.gov/~xiaoye/SuperLU>.

[3] M. H. HOHN, *On the Solution of Mixed Boundary Value Problems in Elasticity*, Ph.D. thesis, Department of Mathematics, University of Utah, Salt Lake City, UT, USA, Dec. 2001. Available at <http://www.math.utah.edu/~hohn/thesis-final.pdf>.

[4] ———, *A little language for modularizing numerical PDE solvers*, Software — Practice and Experience, 34 (2004), pp. 797–813.

[5] A. MORLET ET AL., *The Schwarz alternating sinc domain decomposition method*, Appl. Numer. Math., 25 (1997), pp. 461–483.

[6] F. STENGER, *Numerical Methods Based on Sinc and Analytic Functions*, Springer-Verlag, 1993.

[7] ———, *Summary of sinc approximation*. Available at <http://www.cs.utah.edu/~stenger/PACKAGES/SincPack.ps>, 1993.